ACS OMEGA

http://pubs.acs.org/journal/acsodf

Article

Multispectroscopic and Molecular Docking Insight into Elucidating the Interaction of Irisin with Rivastigmine Tartrate: A Combinational Therapy Approach to Fight Alzheimer's Disease

Rashid Waseem, Anas Shamsi, Taj Mohammad, Fahad A. Alhumaydhi, Syed Naqui Kazim, Md. Imtaiyaz Hassan, Faizan Ahmad, and Asimul Islam*

Cite This: *ACS Omega* 2021, 6, 7910−7921

Read Online

ACCESS | Metrics & More | Article Recommendations | Supporting Information

ABSTRACT: This study was aimed to study the interaction between purified irisin and rivastigmine tartrate (RT), a cholinesterase inhibitor used in Alzheimer's therapy. Irisin mainly promotes brown fat-like features in white adipose tissues; however, it has some important role in the nervous system also, i.e., capable of opposing synapse and memory failure in Alzheimer's disease (AD). The recombinant protein was purified by Ni−NTA chromatography and characterized using spectroscopic and *in silico* techniques. Further, the mechanism of interaction between irisin and RT was investigated using various biophysical techniques. Fluorescence quenching studies suggested that there exists a moderate binding between irisin and RT with a binding constant (K) of 10^4 M^{-1} and the irisin−RT complex is guided by a combination of both static and dynamic modes of quenching. Thermodynamic parameters suggested the reaction to be driven by hydrogen bonding, making it specific. FTIR and CD spectroscopy suggested no secondary structural alterations in irisin in the presence of RT. Molecular docking investigation provided an insight into the important residues that play a key role in irisin−RT interactions. This study delineates an important finding in AD therapy and can provide a platform further to explore the potential of irisin in AD treatment.

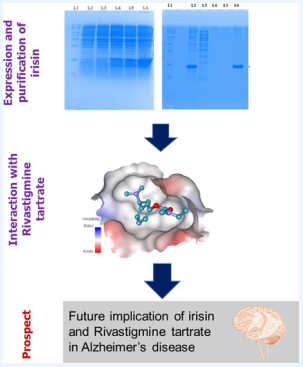

1. INTRODUCTION

Irisin is a recently discovered exercise-induced myokine that is produced after cleavage from the fibronectin type III domain-containing 5 (FNDC5) protein and then secreted into the blood circulation. Irisin is a part of cell membrane protein known as fibronectin type III domain-containing protein 5 (FNDC5/FRCP2/PeP).[1] FNDC5 is made up of a signal peptide, a fibronectin III domain, and a hydrophobic C-terminal domain. FNDC5 is composed of 209 amino acid residues with a N-terminal 29 amino acid-residue signal sequence, followed by fibronectin type III domain (94 amino acid residues), a linking peptide (28 amino acid residues), a transmembrane domain (19 amino acid residues), and a cytoplasmic domain (39 amino acid residues). Human FNDC5 is encoded by the *fndc*5 gene, which spans 10.2 kb size on chromosome locus 1p35.1. The mature peptide of irisin, which is a proteolytically cleaved portion of FNDC5, is of 112 amino acids (32−143 amino acids of FNDC5).[2] Irisin is a hormone, which plays a key role in fat metabolism and the regulation of thermogenesis. It specifically converts the white adipose tissue (WAT) to brown adipose tissue (BAT) through upregulating the expression of an uncoupling protein (UCP1) by increased energy expenditure and weight loss.[2] Irisin is expressed mainly in the heart, liver, brain, skeletal muscles, and salivary glands. Zhang et al. reported that the treatment of recombinant irisin increased the expression of UCP1 through the increased phosphorylation of p38 mitogen-activated protein kinase (p38 MAPK) and other regulatory kinases.[3] Recent studies revealed important biological functions of irisin such as regulation of depression,[4] osteoblast proliferation,[5] and cortical bone mass.[6] There are many other published literature reports that revealed the important role of irisin in the central nervous system.[7] A recent study suggested the expression of irisin by different cell types, namely, Purkinje cells of rodent cerebellum.[8] It was established that irisin induces activation of the Akt and ERK1/2 signaling pathways in brain tissues. Further, it was suggested that the activation of Akt and ERK1/2 might be important for the neuroprotective effects of irisin, as it was supported from other studies where specific chemical inhibitors of the Akt and ERK1/2 pathways abolished the neuro-protection conferred by irisin.[9]

Moreover, many studies have reported that exercise-induced irisin plays a favorable role in brain function and also in neurodegenerative problems such as Alzheimer's disease.[10,11] In the brain, irisin increases the brain-derived neurotrophic factor (BDNF) gene expression, which is a critical regulator of

Received: January 28, 2021
Accepted: February 22, 2021
Published: March 8, 2021

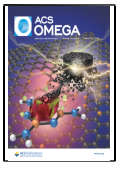

ACS Publications

© 2021 The Authors. Published by American Chemical Society

https://dx.doi.org/10.1021/acsomega.1c00517
ACS Omega 2021, 6, 7910−7921

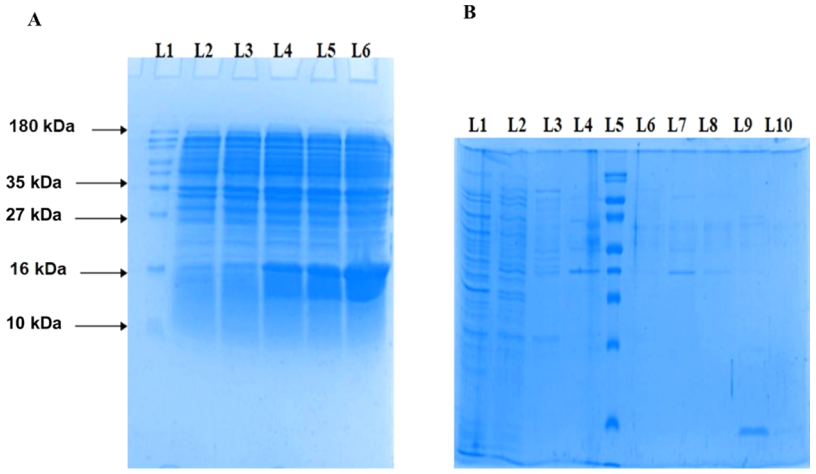

Figure 1. (A) SDS-PAGE gel showing the expression of the irisin protein induced with 0.5 mM IPTG at 37 °C. Lane 1: molecular weight marker; lane 2: uninduced bacterial pellet; lane 3: induced pellet at the 1st hour; lane 4: induced pellet at the 2nd hour; lane 5: induced pellet at the 3rd hour; and lane 6: induced pellet at the 4th hour. (B) SDS-PAGE gel of irisin purification from the supernatant. Lane 1: flow-through after column binding; lanes 2−4: washing with 5, 10, and 50 mM imidazole, respectively; lane 5: molecular mass marker; lanes 6−10: elution with increasing concentration of imidazole (100, 150, 200, 250, and 300 mM, respectively).

neural plasticity.[12] Not only hippocampal BDNF influences neurogenesis, but also hippocampal proliferation is affected by neurogenesis-related signal transducer and activator of transcription 3 (STAT3) signaling.[12] Irisin modulates several AD risk factors,[13] including insulin resistance, impaired neurogenesis, oxidative stress, and imbalance of neurotrophic factors. Irisin shows protective action against the abnormal expression of synapse-related genes, thereby indicating its role in attenuating synaptic and memory impairments in AD mouse models.[14]

Alzheimer's disease (AD) is pathologically characterized by amyloid β (Aβ) plaques, neurofibrillary tangles, and neuronal cell death. A recent study revealed that irisin strongly binds to the specific domain between β-secretase and α-secretase cleavage sites of the amyloid precursor protein (APP). Further, it was proposed that irisin (FNDC5) could suppress the cleavage of β-secretase by binding to the N-terminus of the C99 fragment of APP. Thus, one can speculate that the upregulation of irisin (FNDC5) by exercise may be involved in suppressing Aβ pathology and thus helpful for AD prevention.[15] There are two cholinesterase enzymes that are present in the body, viz., acetylcholinesterase (AChE) and butyrylcholinesterase (BChE). Cholinesterase inhibitors such as rivastigmine tartrate (RT) and donepezil are the "first-line" agents in the treatment of AD. Both rivastigmine tartrate (RT) and donepezil show a dose−response relationship, i.e., the higher the amount of these, the higher the efficacy exhibited by them.[16] Rivastigmine tartrate is a carbamate inhibitor of acetylcholinesterase used for the treatment of mild to moderate Alzheimer's disease in adults[17] and is used under the trade name Exelon.[18]

Thus, to compete with the advancement in the pharmaceutical industries, it is needed to investigate the interaction mechanism of therapeutics and potential drugs with the proteins or target tissues. A lot of proteins, which are either positive or negative regulators of various diseases, are being used as a drug target and therapeutic agents. Therefore, studying protein−drug interactions is important and a major step in pharmacological profiling.

Our study targeted a high yield of purified recombinant irisin in a bacterial system to characterize its biophysical parameters. To date, no literature has reported biophysical characterization of irisin. Pharmacological and pharmacokinetic properties of drugs depend upon their interaction with the carrier protein present in blood plasma.[19] A recent literature has reported the interaction of RT with other important proteins.[20] Rivastigmine is actually a noncompetitive carbamate acetylcholinesterase inhibitor (AChEI), which is structurally different from other currently available inhibitors of acetylcholinesterase enzymes.[21] Some cholinesterase inhibitors such as tacrine and donepezil are known as short-acting or reversible agents because their binding to the acetylcholinesterase (AChE) enzyme is hydrolyzed within minutes.[22] Unlike tacrine and donepezil, rivastigmine is classified as an intermediate-acting, reversible inhibitor, which works by slowly carbamylating the esteratic sites of enzymes.[23] Rivastigmine is sometimes also referred to as a "pseudoirreversible" inhibitor because despite having a very short elimination half-life (2 h), it shows a long inhibition period on AChE of up to 10 h.[23] The next part of this study was to study the binding between irisin and RT, a drug in use for AD therapy. AD is a neurological disorder, which primarily affects memory. It is evident now that memory impairments in AD are caused by synapse failure and loss. Thus, the therapies targeting restoration or preservation of synapse functions and cognition are crucial for AD treatment. It has been found that irisin shows protective action against synapse failure and memory impairments. Moreover, studies have shown the reduced FNDC5/irisin levels in human AD brains and CSF as well as in AD mouse models.[24] Therefore, bolstering brain irisin levels pharmacologically can be a therapeutic strategy to protect or repair synapse functions and prevent cognitive decline in AD. Since RT is an already approved drug for AD treatment, we speculate that administration of RT along with irisin can be a useful therapeutic approach in AD treatment. Currently, various proteins (such as insulin, chimeric proteins, and monoclonal antibodies) are used in clinical treatments, but only a few protein−drug combinations acting on multiple targets have been developed as potential therapies.[25] Combinational therapies have been widely used as clinical treatments for many diseases[26] and have shown to improve therapeutic outcomes as well as ameliorate side effects.[27] However, in

https://dx.doi.org/10.1021/acsomega.1c00517
ACS Omega 2021, 6, 7910−7921

combination therapy, it is necessary to evaluate both the effect of therapeutic protein on the small molecule drug and the effect of drug on the therapeutic protein.[28] Thus, as a preliminary study, the interaction of irisin with RT can serve as a platform for future studies utilizing irisin for AD treatment. This study reveals the formation of a stable complex between irisin and RT.

2. RESULTS

2.1. Expression and Purification. *2.1.1. Expression of Irisin in Bacterial System.* The T7 promoter drives the expression of a cloned fragment, and this is regulated by inducing with isopropyl β-d-thiogalactopyranoside (IPTG), which allows a high level of irisin expression. The confirmed plasmid construct pET15b-irisin was transformed into *Escherichia coli* C41 (DE3) cells (data not shown). Among the transformed colonies of *E. coli*, a solitary colony was isolated and inoculated into 15 mL of LB medium with ampicillin (100 μg) in a 100 mL flask. Post this, flasks were incubated at 37 °C in an orbital shaker at 200 rpm until the optical density reached 0.6 at 600 nm. Then, 1 mL of culture was collected and labeled as an uninduced sample. Figure 1A shows the irisin protein expression profile induced by 0.5 mM IPTG at 37 °C, at an interval of 1 h. Lane 1 is the broad range protein marker, while lane 2 is the uninduced protein (0 h). Lanes 3−6 show the induction of the protein at every 1 h interval. Overexpression of irisin was indicated on SDS-PAGE with an apparent molecular weight of 15−16 kDa (Figure 1A). The figure shows that the induction of 3−4 h is enough for overexpression of the gene.

2.1.2. Purification of Irisin under Native Conditions. In this study, irisin was expressed in *E. coli* C41 (DE3). Under the native condition, the recombinant irisin protein was isolated and purified to homogeneity at 4 °C from the cell extract. Irisin was found in the soluble bacterial extract and obtained after centrifugation of sonicated *E. coli* cells at 10 000*g*. Irisin was purified to homogeneity by single-step chromatography on Ni−NTA affinity chromatography. Fractions of protein obtained in the Ni−NTA affinity chromatography column were subjected to SDS-PAGE to check the purity of the isolated protein. A clear single band was observed on SDS-PAGE, indicating the purity of irisin (Figure 1B, lane 9). As it is apparent from the figure, different concentrations of imidazole were used for elution of the protein of interest bound in the Ni−NTA column. It was found that the protein was eluted at 250 mM imidazole as shown in lane 9 where one can see a single band corresponding to 15.5 kDa (Figure 1B, lane 9). The obtained protein is almost free of any impurities, as evident from the single band on SDS-PAGE.

2.1.3. Purification of Irisin from Inclusion Bodies (IBs). The major portion of the protein was expressed as an insoluble fraction. Since a large portion of the recombinant irisin protein was expressed, it was also purified in the insoluble form exploiting inclusion bodies (IBs). IBs were isolated from the cell extract and purified by sequential washing with Milli-Q water to eliminate contaminants, especially nonspecific proteins and proteases. Purified IBs of 15−16 kDa were checked on SDS-PAGE (Figure 2). Then, 1% *N*-lauroylsarcosine was used to solubilize the IBs. The solubilized IBs were then loaded on a Ni−NTA affinity chromatography column and purified via a single chromatography step. SDS-PAGE was used to check the purity and yield of the fractions (Figure 2).

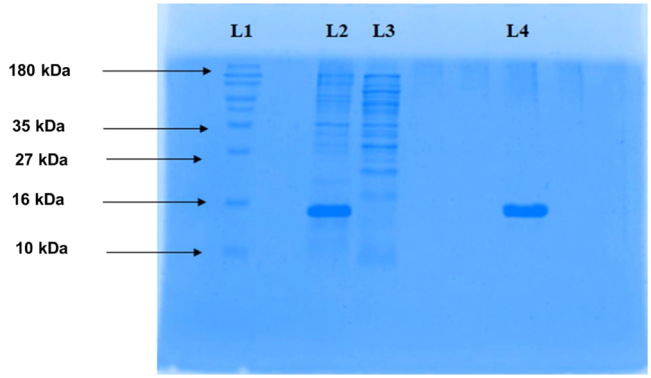

Figure 2. SDS-PAGE gel showing irisin purification from inclusion bodies. Lane 1: molecular mass marker; lane 2: unbound IBs (solubilized in 50 mM Tris buffer, pH 7.5, and 1% *N*-lauroylsarcosine); lane 3: flow-through after column binding; and lane 4: purified irisin obtained after elution with 150 mM imidazole.

2.1.4. Refolding of Irisin. The detergent and the other denaturants or impurities from the protein were removed so that the protein could fold spontaneously into its proper conformation. Although there is no standard protocol for the refolding of proteins, irisin was refolded by dialyzing the solution against 50 mM Tris buffer, pH 7.5, and 300 mM NaCl for 24 h at 4 °C. The dialyzed protein was centrifuged to remove any precipitate formed during refolding. The refolded protein isolated from IBs was subjected to UV, far-UV CD, FTIR, and fluorescence spectroscopic techniques. It is worth mentioning that far-UV CD, FTIR, fluorescence, and UV−vis spectra of the refolded protein isolated under denaturing conditions overlapped with protein purified under native conditions.

2.2. Characterization of Irisin Protein. *2.2.1. Absorption and Fluorescence Spectroscopy.* The UV−vis absorption spectrum of irisin was recorded in the range of 340−240 nm. The spectra obtained showed a peak at 280 nm and a tryptophan hump at 292 nm (Figure 3A). The peak corresponding to 280 nm is a characteristic peak of proteins. Irisin contains two tryptophan residues, and a hump in the UV spectra at 292 nm advocates it to be in a properly folded form. To understand the tryptophan environment of the protein, fluorescence spectral measurements were carried out. Fluorescence emission spectra of irisin showed the emission maximum at 348 nm (Figure 3B). Further, the thermal spectral profile was also recorded to find the melting temperature (T_m) of the isolated protein (Figure 3C), and it was found to be 72 °C.

2.2.2. CD and FTIR Measurements. The purified irisin was used to monitor its secondary structure content using a CD spectropolarimeter. The far-UV CD spectrum of irisin was obtained at pH 7.5 (25 ± 0.1 °C), which provides information regarding the secondary structure. The far-UV CD of irisin showed a negative peak at around 218 nm (Figure 4A), characteristic of a β-sheet-rich protein. FTIR measurements were carried out to substantiate the CD results of the protein. Native irisin showed two peaks, i.e., one peak at around 1646 cm^{-1}, which corresponds to that of water,[29] while the other peak obtained was above 1680 cm^{-1}, which corresponds to an antiparallel β-sheet,[30] which are characteristic features of native irisin (Figure 4B).

Irisin stimulates the expression of the brain-derived neurotrophic factor (BDNF) in the hippocampus, a brain

https://dx.doi.org/10.1021/acsomega.1c00517
ACS Omega 2021, 6, 7910−7921

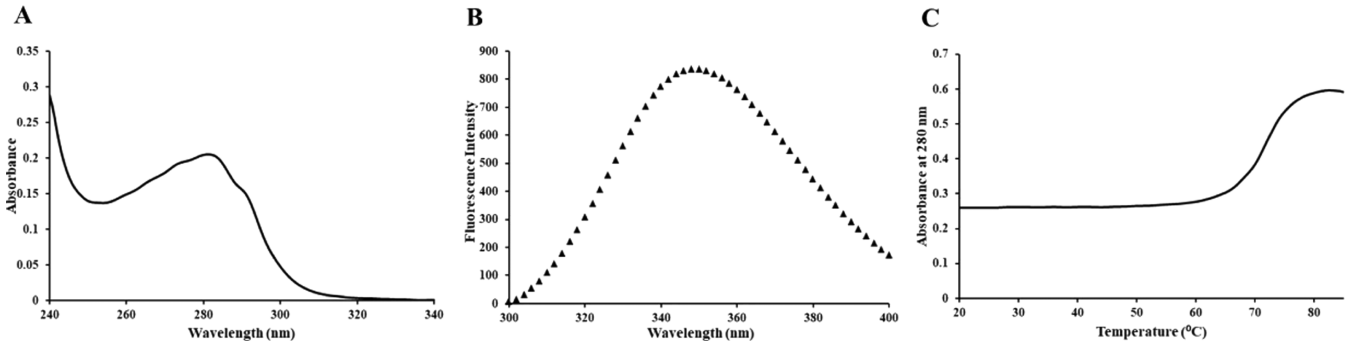

Figure 3. (A) Near-UV absorbance spectrum of native irisin. (B) Fluorescence spectrum of native irisin. (C) Heat-induced denaturation profile of native irisin.

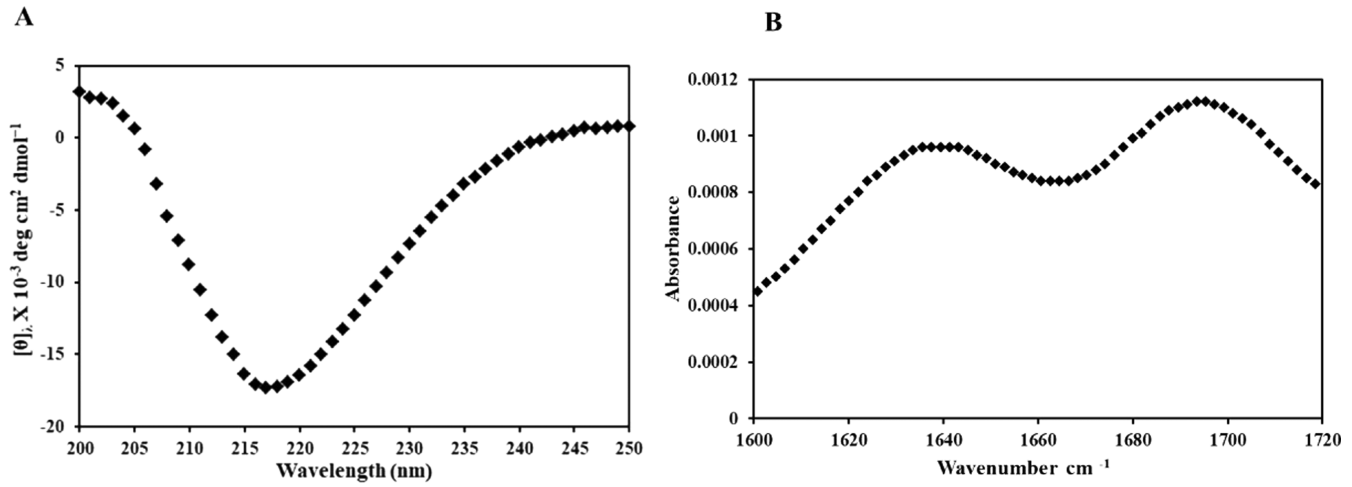

Figure 4. (A) Far-UV CD spectrum of native irisin. The recording range was 200−250 nm. (B) FTIR spectrum of native irisin.

region centrally involved in learning and memory.[31] This raises the possibility that irisin could play a neuroprotective role in brain disorders such as Alzheimer's disease (AD). Further, irisin levels are reduced in AD hippocampi and the cerebrospinal fluid.[14] This strong correlation between AD and irisin led us to ponder what may be the effect of AD's drug on the structure of irisin. Rivastigmine tartrate (RT) is often used for the treatment of mild to moderate Alzheimer's disease in adults. We have characterized the structure of irisin in the presence of RT.

2.3. Interaction Study between Purified Irisin and Rivastigmine Tartrate. *2.3.1. Steady-State Fluorescence.* Fluorescence spectroscopy is a technique that is often employed to have an insight into the interaction between a protein and a drug as this gives the indication of changes around aromatic residues of proteins.[32,33] Herein, fluorescence spectroscopy was employed to investigate the complex formation between irisin and rivastigmine tartrate (RT). Irisin has one tyrosine (Tyr98) and two tryptophan residues (Trp51, Trp90). Due to Trp residues, irisin shows a strong fluorescence emission peak at 348 nm when excited at 280 nm. A substantial decrease in the fluorescence intensity of irisin with increasing concentrations of RT suggested a moderate binding affinity between irisin and RT (Figure 5A,B). Temperature dependence of binding parameters gives a clue about the type of quenching taking place for the protein−ligand interaction and, thus, fluorescence measurements were carried out at three different temperatures.[34] Fluorescence quenching is a phenomenon in which a wide variety of small molecules or ions act as quenchers of fluorescence, i.e., they decrease the intensity of the emission.[35,36] This quenching can be either static, dynamic, or combined dynamic and static quenching caused by both collision and complex formation with the same quencher, respectively.[37−39] Fluorescence quenching is mathematically evaluated by applying various equations to find out quenching and binding parameters. The quenching data was fitted to eqs 1−3 to obtain different parameters for the irisin−RT interaction as per previously published studies.[40,41]

Stern−Volmer plots of irisin quenching in the presence of varying concentrations of RT are depicted in Figure 5C; the slope of this plot as per eq 1 gives the value of Stern−Volmer constant (K_{sv}).[42] The plot of F_0/F against $[C]$ at 20, 28 and 34 °C slightly deviates from linearity toward the *y*-axis, suggesting that combined static and dynamic quenching guides irisin−RT interactions.[43]

The variation in K_{sv} values at different temperatures can be suggestive of the type of quenching taking place for specific drug−protein interactions.[34] K_{sv} was obtained at three different temperatures and was found to increase with an increase in temperature, implying that dynamic quenching governs irisin−RT interactions[44] (Table 1). Table 1 shows values of K_{sv} for irisin−RT interactions at different temperatures.

The value of K_q for irisin−RT interactions was calculated using eq 2 and was found to be substantially higher than the maximum scatter collision quenching constant of various quenchers with biopolymers (2×10^{10} M^{-1} s^{-1}),[20] indicating that static quenching effect may also exist in the irisin−RT system.[37] Presence of static quenching implies the formation of

https://dx.doi.org/10.1021/acsomega.1c00517
ACS Omega 2021, 6, 7910−7921

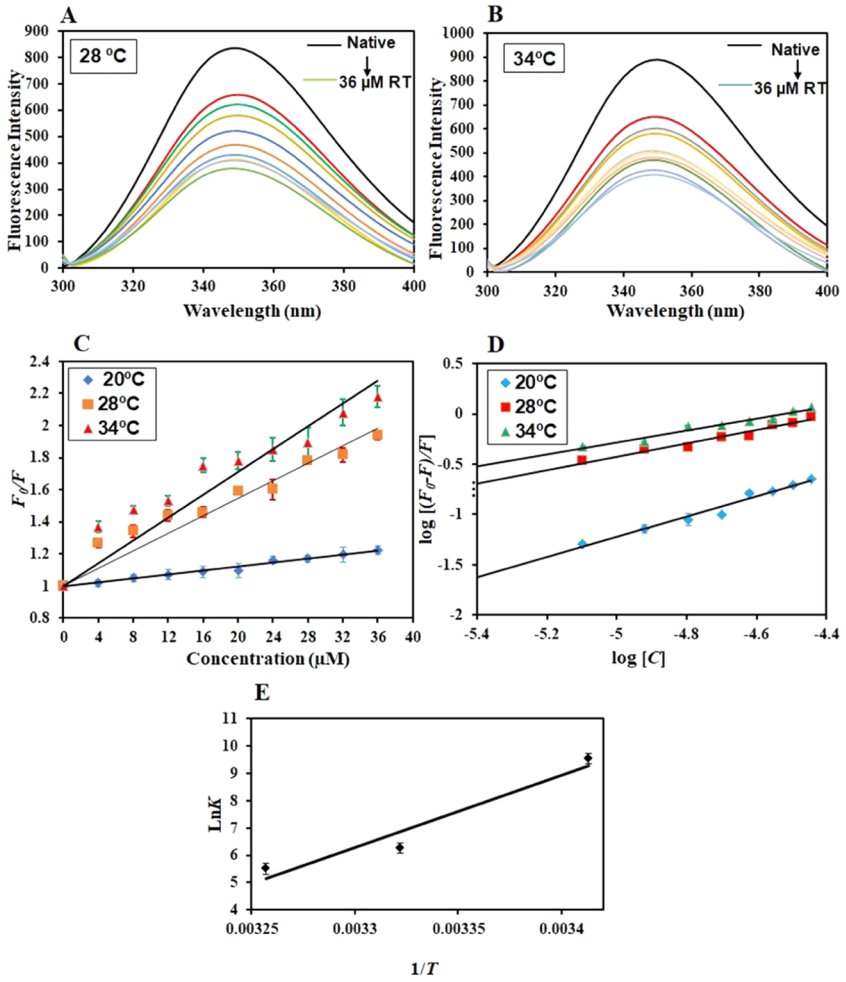

Figure 5. Steady-state fluorescence of irisin in the presence of a varying concentration of RT (4−36 μM) at (A) 28 °C and (B) 34 °C. (C) Stern−Volmer plot of irisin with varying RT concentration (4−36 μM) at three different temperatures (20, 28, and 34 °C). (D) Double log relation of irisin−RT at three different temperatures. (E) Van 't Hoff plot having ln K on the Y-axis and $1/T$ on the X-axis.

Table 1. Thermodynamic Parameters Obtained for Irisin−RT Interactions

temperature (°C)	K_{sv} (10^4 M^{-1})	K_q (10^{12} M^{-1} s^{-1})	R^2
20	0.6	0.22	0.98
28	2.7	1.00	0.96
34	3.5	1.29	0.94

a nonfluorescent complex in the RT−irisin complexation process.[45] Thus, it can be said that the irisin−RT interaction is initiated by a combined quenching process including both dynamic and static quenching.[37]

The binding constant was estimated using eq 3 as per other studies where both quenching were found to be operative for protein−ligand interactions.[37] Figure 5D shows the fitting of the data as per eq 3 with the intercept of the plot giving the value of the binding constant (K) and the slope depicting the number of binding sites (n). The value of K was found to be 1.3×10^4 M^{-1} at 20 °C, indicating moderate binding between irisin and RT as has been reported for other protein−ligand interactions.[46] Table 2 shows the K obtained at different temperatures, suggesting that a less stable complex is formed at higher temperatures as the value of K decreases at higher temperature.

Thermodynamic parameters of any reaction depict the feasibility of the reaction and also give an idea about the type of forces that play a role in complex formation between a protein and a ligand.[38] After investigating the binding parameters of irisin−RT interactions, the next aim was to find out the thermodynamic parameters associated with the interaction. The van 't Hoff equation (eq 4) is deployed to calculate these parameters, viz., Gibbs free energy (ΔG), enthalpy change (ΔH), and entropy change (ΔS). The van 't Hoff plot is a plot having ln K on the Y-axis with the inverse of temperature on the X-axis. The slope of this plot gives $-\Delta H/R$ with the intercept giving $\Delta S/R$. Figure 5E depicts the van't

Table 2. Thermodynamic Parameters Obtained for Irisin−RT Interactions

temperature (°C)	K (10^4 M^{-1})	n	ΔG (kcal mol^{-1})	ΔS (cal mol^{-1} K^{-1})	ΔH (kcal mol^{-1})	$T\Delta S$ (kcal mol^{-1})
20	1.3	1.07	−5.39596	−52.76	−161.652	−47.364
28	0.05	0.66	−4.10274			−48.6573
34	0.02	0.6	−3.13283			−49.6272

https://dx.doi.org/10.1021/acsomega.1c00517
ACS Omega 2021, 6, 7910−7921

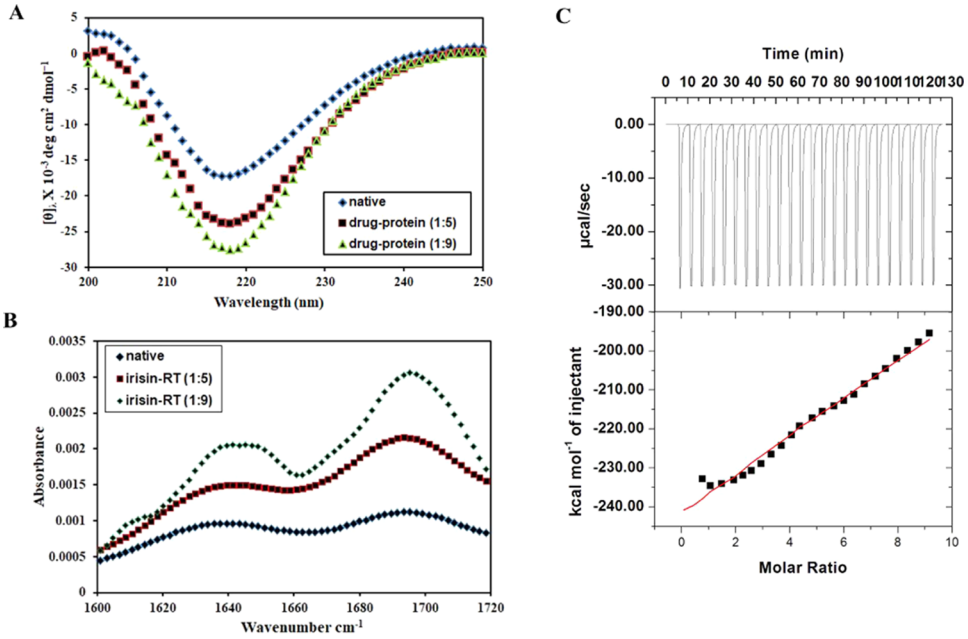

Figure 6. (A) Far-UV CD spectra of irisin in the absence and presence of RT (1:5 and 1:9). (B) FTIR spectra of irisin in the absence and presence of RT (1:5 and 1:9). (C) ITC profile of irisin−RT interactions. Each downward peak in the upper panel shows changes in heat accompanying each titration. The lower panel shows an integrated plot of the amount of heat liberated per injection as a function of the molar ratio of RT to irisin.

Hoff plot for irisin−RT interactions. Thermodynamic parameters obtained for irisin−RT interactions are depicted in Table 2.

The negative Gibbs free energy obtained depicts the spontaneous nature of this reaction.[47] On the other hand, the negative values of enthalpy and entropy obtained suggest the exothermic nature of the reaction and the fact that the irisin−RT interaction is enthalpy-driven and not entropy-driven. There are mainly four prevailing interaction forces, viz., van der Waals force, electrostatic force, hydrophobic interactions, and hydrogen bonding.[42] It is a known and well-established fact that negative enthalpy and entropy suggest hydrogen bonding and/or van der Waals dominance, whereas positive enthalpy and entropy changes suggest the existence of hydrophobic interactions. Thus, it can be concluded that for the irisin−RT interaction, hydrogen bonds and van der Waals forces are prevalent with reaction being enthalpy-driven.

2.3.2. UV−Vis Spectroscopy. UV−vis absorption measurement is a simple and effective method for studying the interactions of the structure change and formation of a complex of protein with small molecules. The UV−vis absorption spectrum of irisin was measured in the presence of RT in the range 340−240 nm. As shown in Figure SI, there was a change in the intensity of the absorption band of irisin at around 280 nm in the presence of RT as compared to free irisin. The increase in the intensity of the absorption band in the presence of RT can be attributed to irisin−RT complex formation.

2.3.3. Circular Dichroism (CD). CD is an informative and rapid spectroscopic technique for studying the secondary structure, binding properties, and conformational changes that occur during the folding and unfolding of the proteins.[48] For studying the effect of a drug on a protein, CD spectroscopy may be exploited. CD spectroscopy depicts conformational changes in a protein upon addition of a ligand. The CD spectrum of α-helix-rich proteins shows peaks at around 208 and 222 nm, while the CD spectrum of β-sheet-rich proteins shows a peak at around 218 nm.[49] Figure 6A shows far-UV CD spectra of irisin in the absence and presence of RT. Native irisin shows a peak at 218 nm, which is characteristic of β-sheet. In the presence of RT (1:5 and 1:9), there is an evident downward movement of CD spectra with no significant peak shift. The maximum increase was observed for irisin−RT (1:9). This downward movement of CD spectra with no peak shift suggests that complex formation may be taking place between irisin and RT.

2.3.4. FTIR Spectroscopy. Further, to validate the CD spectroscopy results, FTIR spectroscopy was carried out. Amide I is the most intense absorption band in proteins, C═O (70−85%) and C−N groups (10−20%) being the key players. The amide I range is 1600−1700 cm^{-1}, and this is the region that is exploited for studying secondary structural alterations. Figure 6B shows FTIR spectra of irisin in the absence and presence of RT (1:5 and 1:9), and it is quite apparent that there is no significant change in peak and only change in intensity in the presence of RT, which is consistent with CD spectroscopy observations. Thus, CD spectroscopy coupled with FTIR spectroscopy advocates the complex formation between irisin and RT.

2.3.5. Isothermal Titration Calorimetry. To complement fluorescence binding studies, ITC was further deployed to ascertain binding affinity between irisin and RT and find associated thermodynamic parameters. Figure 6C shows the ITC isotherm of irisin titrated with RT. Every peak of the binding isotherm represents a single injection of RT into the recombinant irisin solution filled in the sample cell. The lower panel corresponds to heat liberated per injection as a function of the molar ratio of RT to irisin. This data was obtained for the model of one binding site. The thermodynamic parameters obtained for irisin−RT interactions were as follows: K_a = 69.3 ± 2.34 × 10^3 M^{-1}, ΔH = −5.01 × 10^5 ± 6.81 × 10^5 cal/mol, and ΔS = −1.67 × 10^3 cal/mol/deg. There may be variations in thermodynamic parameters obtained from fluorescence

https://dx.doi.org/10.1021/acsomega.1c00517
ACS Omega 2021, 6, 7910−7921

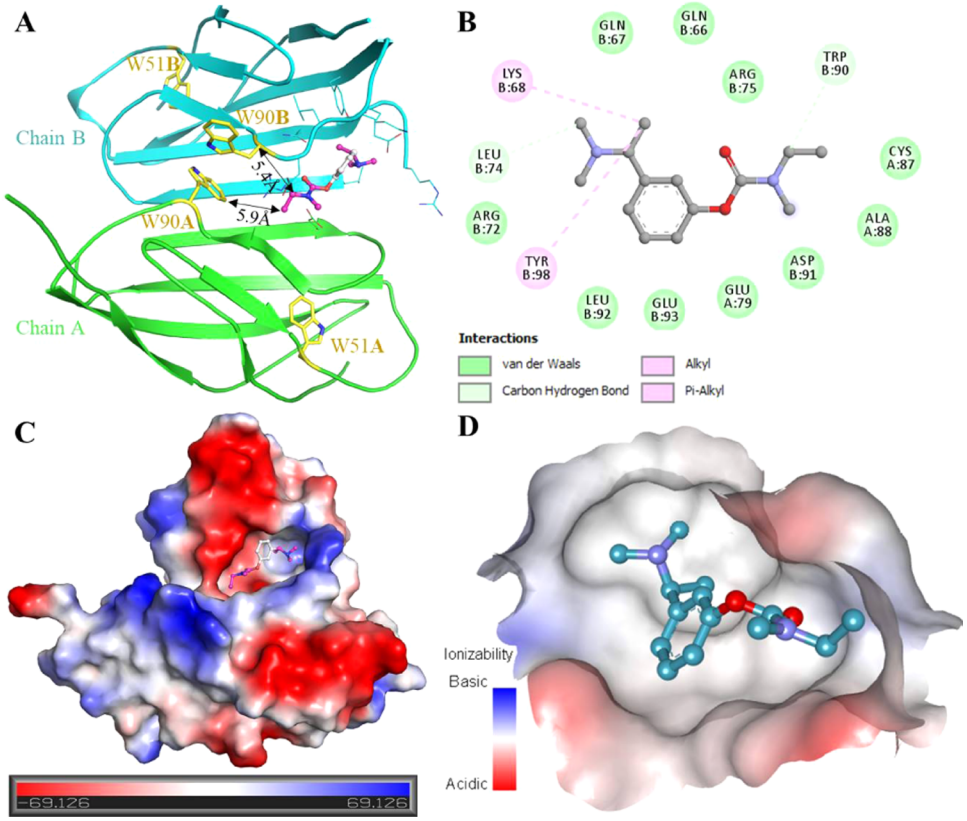

Figure 7. Interactions of RT with irisin. (A) Structural representation of irisin bound with docked RT. (B) 2D structural representation of irisin residues interacting with RT. (C) Surface-potential representation of irisin showing the docked RT in the deep binding cavity. (D) Zoomed surface view of the irisin binding pocket occupied by RT.

spectroscopy and ITC owing to assumptions made that the enthalpy change is not temperature-dependent.[50,51] The negative value of ΔG affirms the spontaneous nature of this reaction. These observations corroborate with fluorescence spectroscopy observations, affirming that RT binds to irisin with significant affinity.

2.3.6. Molecular Docking Analysis. Molecular docking provided mechanistic details of irisin−RT interactions at a molecular level, which aided in exploring their binding pattern that further support in identifying the interacting residues and calculating the affinity score. The predicted affinity was estimated as −5.4 kcal/mol for RT with irisin, which is quite significant while considering the ligand efficiency (LE) of RT that is 0.3 kcal mol^{-1} non-H $atom^{-1}$. The p*Ki* value of RT−irisin was obtained as 3.96. Figure 7A shows the irisin dimer depicted as a ribbon diagram in complex with docked RT, which is shown in the ball and sticks model. Figure 7B gives a detailed analysis of all of the key residues of the irisin binding pocket that are involved in different kinds of interactions, thereby playing a role in irisin−RT complex formation. Figure 7C,D shows that RT is placed in the deep cavity of the irisin binding pocket. Thus, these *in silico* observations further validate the *in vitro* results advocating the binding of RT with irisin, leading to complex formation.

3. DISCUSSION

Initially, irisin was revealed as an exercise-induced myokine catalyzing the conversion of WAT to BAT and thereby increasing thermogenesis.[2] However, with time, the knowledge pertaining to different roles of irisin has evolved and, unlike earlier, irisin is no more confined to fat browning and thermogenesis. Recently, several debates concerning nature and irisin identity popped up, but several sensitive approaches confirmed the identity of irisin and also gave a measure of its circulating levels in humans.[52,53] In the present study, the recombinant human irisin was successfully expressed and purified in a bacterial system in both native and denatured conditions. Irisin was purified using Ni−NTA affinity chromatography. Under native conditions, the protein was pure and homogeneous, but the yield was very low. To increase the yield, an alternate method was employed. IBs were prepared, and irisin was purified from them under denaturing conditions. Homogenized solubilized inclusion bodies (IBs) having 1% *N*-lauroylsarcosine were used to purify the protein through Ni−NTA chromatography (single-step purification) and refolded into the biologically active form. The pure protein coupled with high concentration was obtained through this procedure, thus concluding that purification of irisin from its IBs under denatured conditions was a good approach. The expression and purification procedures reported in this study provide a simple and efficient method to obtain a pure irisin protein, which is highly unexplored in many aspects, thus making this study relevant. The purified protein was further subjected to its biophysical characterization using different spectroscopic techniques. Biological macromolecules such as proteins and nucleic acids absorb light in the UV−visible region of the spectrum. The wavelength of absorption and the strength of absorbance of a molecule depend not only on the chemical nature but also on the molecular environment of its chromophores. Absorption spectroscopy is therefore an

https://dx.doi.org/10.1021/acsomega.1c00517
ACS Omega 2021, 6, 7910−7921

excellent technique for following ligand-binding reactions, enzyme catalysis, and conformational transitions in proteins and nucleic acids. Spectroscopic measurements are very sensitive and nondestructive and require only small amounts of material for analysis. The aromatic side chains of Tyr, Trp, and Phe absorb light in the 240−300 nm region, where λ_{max} is 280 nm for Trp, 275 nm for Tyr, and 257 nm for Phe. In the near-UV region, the molar absorbance of phenylalanine is much smaller than that of tyrosine and tryptophan, and the spectrum of a protein between 240 and 300 nm is therefore dominated by the contributions from the Tyr and Trp side chains. Phe residues contribute a fine structure ("wiggles") to the spectrum between 250 and 260 nm. The aromatic amino acids do not absorb above 310 nm, and therefore protein absorbance should be zero at wavelengths greater than 310 nm. The UV spectral profile showed that the purified protein is properly folded with a characteristic peak at around 280 nm coupled with a tryptophan hump at 292 nm as irisin has two Trp residues. Native proteins can be unfolded by heat. Protein unfolding transitions can thus be measured by following the absorbance changes at 287−292 nm as a function of temperature. The refractive index decreases slightly with temperature, as well as the protein concentration (due to the thermal expansion of the solution), and the ionization of dissociable groups can change. Altogether, these effects influence protein absorbance only to a minor extent and therefore the dependence on temperature is usually small in the absence of structural transitions. To determine the stability of the protein, we performed heat-induced denaturation, and the T_m of irisin was found to be 72 °C.[48,54−56]

Fluorescence spectroscopy was exploited, which showed a peak at 348 nm, which is again indicative of a folded protein. The secondary structure analysis was carried out employing CD and FTIR spectroscopy techniques. The far-UV CD spectrum of native irisin showed a negative peak at 218 nm, which is a characteristic of the β-pleated sheet structure. The CD spectra of β sheets are less intense than those of helices, and they display a single negative band near 217 nm, although the position can vary by up to 5 nm. FTIR spectra also showed a peak above 1680 cm^{-1} that corresponds to antiparallel β-sheet, thus confirming the existence of the β-sheet structure in native irisin.

Irisin has a protective role in both the central and the peripheral nervous systems, including the regulation of brain-derived neurotrophic factors. A recent study has reported that boosting brain levels of FNDC/irisin rescued synaptic plasticity and memory in AD models and that irisin is an important mediator of the beneficial effects of exercise on synaptic plasticity and memory in AD models.[14] The next part of study provided an insight into the binding mechanism of irisin with RT, a cholinesterase inhibitor that is used in AD treatment. Irisin is a potential therapeutic agent against AD;[12] hence, understanding the interaction of irisin with RT and elucidation of molecular mechanisms underlying this interaction can be beneficial in several ways.

The binding parameters of the RT−irisin complex were explored by performing an intrinsic fluorescence assay at varying temperatures (20, 28, and 34 °C). Fluorescence quenching studies discovered that the irisin−RT interaction is initiated by a combined quenching process exploiting both dynamic and static quenching. Thermodynamic parameters were also found using the van 't Hoff equation, and the negative values of ΔH and ΔS suggested this reaction to be driven by hydrogen bonding and/or van der Waals forces with negative ΔG showing the reaction to be spontaneous. The spontaneity was further affirmed by the ITC profile of irisin−RT interactions. CD spectra of free irisin and the RT−irisin complex indicate that RT induces minimal structural changes in irisin as there was no peak shift; however, there was an upward movement in CD spectra of the irisin−RT complex, suggesting the complex formation with no effect of RT on the secondary structure of irisin.[57] FTIR results further complement the CD spectroscopy observations as there was no peak shift in the FTIR spectra of the irisin−RT complex as compared to native irisin.

The findings of this study can be of significant benefit to Alzheimer's therapy along with new prospects to the field of clinical medicine as irisin is a potential therapeutic agent capable of ameliorating AD neuropathology. As this field is least explored and this work is a first of its kind, this investigation is an important novel approach. Bolstering brain irisin levels pharmacologically can be a therapeutic strategy to protect or repair the synapse function and prevent cognitive decline in AD. Since RT is an already approved drug for AD treatment, we speculate that administration of RT along with irisin can be a useful therapeutic approach in AD treatment. Irisin is a recently identified protein that is largely unexplored in many ways and hence this study can serve as a platform for future studies utilizing irisin along with RT as a potential therapeutic agent against AD.

4. MATERIALS AND METHODS

The expression construct of irisin (pET15b-His-3C-irisin) (Uniprot ID: Q8NAU1, seq. 32−143) was purchased from Addgene (122612). The C41 (DE3) strain of *E. coli* was used for the expression of the protein. *E. coli* cells harboring recombinant plasmids were grown aerobically at 37 °C in Luria−Bertani (Merck, Darmstadt, Germany) broth with 100 μg/mL ampicillin (Sigma, Saint Louis, MO).[58] Plasmid isolation and competent cell preparation were carried out using standard procedures.[58]

4.1. Expression of the Protein. The constructed expression vector (pET15b-irisin) comprising the coding region of the irisin gene was transformed into *E. coli* C41 (DE3) host cells by following a standard protocol (20). The overnight culture of the expression cells from a freshly transformed plate was used for secondary culture, and induction of irisin expression was carried out using 0.50 mM IPTG followed by incubation for the next 4 h at 37 °C. The fully grown culture was subjected to centrifugation at 7000*g* for 15 min at 4 °C, followed by incubation with lysis buffer (50 mM Tris−HCl buffer, pH 7.5, containing 300 mM NaCl, 5% (v/v) glycerol, 0.5 mM β-mercaptoethanol, and 100 mM phenyl methane sulfonyl fluoride (PMSF)). The cell lysate was sonicated on ice, and after centrifugation, the supernatant was collected for purification of irisin by nickel affinity chromatography.

4.2. Protein Purification. The Ni−NTA column was first pre-equilibrated with buffer X (25 mM Tris−HCl, pH 7.5, 300 mM NaCl, 5% (v/v) glycerol, 0.5 mM β-mercaptoethanol) and 5 mM imidazole. Then, the supernatant was passed through the column. After binding of protein, the column was washed with 100 mL of washing buffer (buffer X + 10 mM imidazole) at 4 °C. The bound protein was eluted with different concentrations of imidazole (50−300 mM) and dialyzed against 50 mM Tris−HCl pH 7.5 buffer. Sodium dodecyl

https://dx.doi.org/10.1021/acsomega.1c00517
ACS Omega 2021, 6, 7910−7921

sulfate-polyacrylamide gel electrophoresis (SDS-PAGE) was done to confirm the purity of the protein.

4.3. Alternative Methods of Irisin Purification. The major portion of irisin was expressed as insoluble protein in the form of inclusion bodies (IBs), so an alternative method of irisin purification is also reported here. The yield of the protein that we purified from the soluble fraction was very low. To increase the yield of irisin protein, several different methods were tried to isolate the protein from IBs.

4.4. Preparation and Solubilization of IBs. *E. coli* cells were centrifuged, and after centrifugation, pellets were resuspended in lysis buffer (50 mM Tris buffer and 300 mM NaCl, pH 7.5) and lysed through sonication. After low-speed centrifugation, the pellet was again resuspended and washed with Milli-Q water through centrifugation thrice to remove contaminations and thus purified IBs were obtained. Purified IBs were solubilized with solubilization buffer (50 mM Tris buffer pH 7.5, 300 mM NaCl, and 1% *N*-lauroylsarcosine) and incubated on a rocker for 30 min. The solubilized IBs were centrifuged for 30 min at 9000 rpm, and the supernatant was collected.

4.5. Purification of Recombinant Irisin from IBs. The Ni−NTA column was equilibrated with equilibration buffer, and the collected supernatant was loaded on the equilibrated Ni−NTA column. Then, the column was washed with washing buffer (equilibration buffer + 20 mM imidazole) and the desired protein was eluted with elution buffer (buffer Y) with different concentrations of imidazole. The fractions of the eluted irisin protein were collected and checked for homogeneity on SDS-PAGE.

4.6. Measurement of Absorption Spectra. The absorption spectrum of the irisin protein was measured by a JASCO UV-660 UV/Vis spectrophotometer whose temperature was maintained by circulating water from an external refrigerated water bath. Then, 4 μM protein was used for performing absorption measurements. All measurements were carried out using a 1 cm path length cuvette in the wavelength range of 240−340 nm. All spectral measurements were done three times, and the temperature was fixed at 25 ± 0.1 °C. Further, near-UV spectra of the protein were measured in the presence of different concentrations of the drug. All of these experiments were carried out in 50 mM Tris−HCl buffer, pH 7.5.

4.7. Measurement of Thermal Denaturation Transition Curve. Thermal denaturation studies were carried out using a JASCO UV-660 UV/Vis spectrophotometer where the temperature was controlled by a programmable Peltier-type (ETCS-761) temperature controller interfaced with a personal computer. Then, 4 μM protein solution was heated at a rate of 1 °C/min from 20 to 85 °C by placing the cuvette in the cell holder attached to the Peltier-type temperature controller. The protein solution was heated to a temperature just a few degrees above the temperature where complete denaturation was achieved and then cooled back to 25 °C. This was done to check the reversibility of thermal denaturation curves. The optical properties were measured again and compared with those of the native protein. Each measurement was carried out at least three times, and the baseline was corrected by the buffer in question.

4.8. Fluorescence-Based Binding Assay. To study the binding affinity of RT with the recombinant irisin, the fluorescence-based binding study was carried out and analyzed as described earlier.[20,34] The dilution of the stock solution of RT to working concentration was achieved with double distilled water, while the protein dilution was done with the last dialysis buffer. The protein was excited at 280 nm with emission recorded in the range of 300−400 nm and with both excitation emission slits set at 10 nm, on medium range.

Fluorescence quenching of irisin with an increasing concentration of RT was mathematically investigated employing the Stern−Volmer equation (eq 1), eq 2, and modified Stern−Volmer equation (eq 3) as in previous studies[59,60] to estimate different binding parameters.

$$\frac{F_0}{F} = 1 + K_{sv}[C] \tag{1}$$

F_0 and F refer to the intensity of free irisin and irisin in the presence of RT. $[C]$ refers to varying concentrations of RT. K_{sv} is the obtained Stern−Volmer constant.

Equation 2 uses K_{sv} to confirm the operative mode of quenching for the protein−ligand interaction.

$$K_q = \frac{K_{sv}}{\tau_0} \tag{2}$$

τ_0 is the average integral fluorescence lifetime of tryptophan (2.7×10^{-9} s),[20] which is used to find the bimolecular quenching rate constant (K_q).

$$\log \frac{F_0 - F}{F} = \log K + n \log[C] \tag{3}$$

K denotes the "binding constant of the irisin−RT complex", while "n" shows the number of binding sites and C shows the concentration of RT. It should be noted that all of these experiments were carried out in 50 mM Tris−HCl buffer, pH 7.5.

The van 't Hoff equation[61] (eq 4) is used to find the associated thermodynamic parameters for a reaction with the slope of the van 't Hoff plot ($\ln K$ on the Y-axis against $1/T$ on the X-axis) giving the value of $-\Delta H/R$ and the intercept giving the value of $\Delta S/R$. The magnitude and values of these parameters serve as the guiding light to find the forces that drive the reaction.

$$\Delta G = -RT \ln K = \Delta H - T\Delta S \tag{4}$$

K is the obtained binding constant, ΔH is the associated enthalpy change, and ΔG is the associated free Gibbs energy change. ΔS denotes the associated entropy change with reaction, and R is the universal gas constant.

4.9. Circular Dichroism (CD). The secondary structure of irisin was measured using circular dichroism (CD) in a JASCO spectropolarimeter (model J-1500) equipped with a Peltier-type temperature controller. The far-UV CD spectra (250−200 nm) were recorded at 25 ± 0.1 °C using a cuvette of 1 mm path length cell with a scanning rate of 100 nm/min and protein concentration of 8 μM. The sample of the native irisin was prepared in 25 mM Tris−HCl containing 100 mM NaCl at pH 7.5. CD data was transformed into a concentration-independent parameter $[\theta]_\lambda$ (deg cm^2 dmol^{-1}), the mean residue ellipticity (MRE) as per previous studies

$$[\theta]_\lambda = \frac{M_o \theta_\lambda}{10XlXC}$$

where θ_λ is the ellipticity in millidegrees at wavelength λ, M_o is the mean residue weight of the protein, C is the protein concentration, and l is the cell path length in centimeters.

https://dx.doi.org/10.1021/acsomega.1c00517
ACS Omega 2021, 6, 7910−7921

Further, far-UV CD spectra of the protein were measured in the presence of different concentrations of RT.

4.10. Infrared Spectroscopy Measurements. Fourier transform infrared (FTIR) spectral measurements were done using Agilent Technologies Carry 630 FTIR fitted to a MICROTEK with an MCT detector. The concentration of irisin was 8 μM in 25 mM Tris buffer, pH 7.5. Initially, a diamond window was used for pipetting the samples, and then, 100 scans were obtained for each background. The spectra were obtained with a supposed resolution of 2 cm^{-1} at 25 °C. To get normalized spectra, all infrared spectra were rescaled in the range 1600−1720 cm^{-1}.

4.11. Isothermal Titration Calorimetry (ITC) Measurements. A VP-ITC microcalorimeter from MicroCal, Inc. (GE, MicroCal) was employed to perform isothermal titration calorimetry (ITC) measurements as per previously published protocols.[57,62] The sample cell contained 20 μM irisin, while the syringe was filled with 1 mM RT. There was a programmed titration in which the first injection was false; this was of 2 μL, while the following injections were of 10 μL and the stirring rate was 320 rpm. Data analysis was carried out using the attached MicroCal Origin 8.0 package.

4.12. Molecular Docking. Molecular docking analysis of irisin with RT was carried out to see the interaction pattern. Bioinformatics software packages, such as MGLTools,[63] AutoDock Vina,[64] PyMOL,[65] and Discovery Studio,[66] were used in docking and analysis. Atomic coordinates of irisin were obtained from the Protein Data Bank (PDB ID: 4LSD). Receptor preparation was done while using the AutoDockTools by adding missing polar atoms and assigning appropriate atom types. The PDB file format was converted into the AutoDock standard file format PDBQT. The three-dimensional structure of RT was obtained from the PubChem database. We have used InstaDock, a newly developed program for molecular docking that uses QuickVina-W in docking calculations, which is created by modifying the search strategy of AutoDock Vina modifying neither the scoring function nor the interface.[67] This program gives multiple parameters for protein−ligand interactions including ligand efficiency, which is a commonly applied parameter for selecting promising small molecules by comparing the values of average binding energy per atom.[68]

We have also calculated the inhibition constant (pKi), which is a negative decimal logarithm of the inhibition constant that comes from the ΔG parameter of the docking result. The pKi value of both compounds was calculated using the following formula

$$\Delta G = RT\ (\ln Ki_{\text{pred}})$$

$$Ki_{\text{pred}} = e^{(\Delta G/RT)}$$

$$pK_i = -\log(Ki_{\text{pred}})$$

where ΔG is the binding affinity (kcal/mol); R is the gas constant, 1.98 cal·(mol·K)$^{-1}$; T is the room temperature, 298.15 K; and pred denotes predicted.

Ligand efficiency (LE) is a commonly applied parameter for selecting promising molecules by comparing the values of average binding energy per atom. The following formula was applied to calculate LE

$$LE = -\Delta G/N$$

where LE is the ligand efficiency (kcal mol^{-1} non-H $atom^{-1}$), ΔG is the binding affinity (kcal mol^{-1}), and N is the number of non-hydrogen atoms in the ligand.

■ ASSOCIATED CONTENT

Supporting Information

The Supporting Information is available free of charge at https://pubs.acs.org/doi/10.1021/acsomega.1c00517.

UV spectra of irisin in the absence and presence of RT (1:9) (Figure SI) (PDF)

■ AUTHOR INFORMATION

Corresponding Author

Asimul Islam − *Center for Interdisciplinary Research in Basic Sciences, Jamia Millia Islamia, New Delhi 110025, India;* orcid.org/0000-0001-9060-7970; Phone: +91-9312812007; Email: aislam@jmi.ac.in

Authors

Rashid Waseem − *Center for Interdisciplinary Research in Basic Sciences, Jamia Millia Islamia, New Delhi 110025, India*

Anas Shamsi − *Center for Interdisciplinary Research in Basic Sciences, Jamia Millia Islamia, New Delhi 110025, India;* orcid.org/0000-0001-7055-7056

Taj Mohammad − *Center for Interdisciplinary Research in Basic Sciences, Jamia Millia Islamia, New Delhi 110025, India*

Fahad A. Alhumaydhi − *Department of Medical Laboratories, College of Applied Medical Sciences, Qassim University, Buraydah 52571, Saudi Arabia;* orcid.org/0000-0002-0151-8309

Syed Naqui Kazim − *Center for Interdisciplinary Research in Basic Sciences, Jamia Millia Islamia, New Delhi 110025, India*

Md. Imtaiyaz Hassan − *Center for Interdisciplinary Research in Basic Sciences, Jamia Millia Islamia, New Delhi 110025, India;* orcid.org/0000-0002-3663-4940

Faizan Ahmad − *Center for Interdisciplinary Research in Basic Sciences, Jamia Millia Islamia, New Delhi 110025, India*

Complete contact information is available at: https://pubs.acs.org/10.1021/acsomega.1c00517

Notes

The authors declare no competing financial interest.

■ ACKNOWLEDGMENTS

This work was supported by the grant from the Indian Council of Medical Research (ICMR)BIC/12(16)/2014. For the award of Senior Scientist Position, F.A. is thankful to the Indian National Science Academy. The authors are grateful to FIST Program (SR/FST/LSI-541/2012) and Jamia Millia Islamia (a Central University) for providing all of the necessary facilities to carry out this work. R.W. acknowledges DST-INSPIRE for INSPIRE Fellowship (IF-180728). A.S. is thankful to UGC for D.S. Kothari Postdoctoral fellowship ((BSR)/BL/19-20/0119).

■ ABBREVIATIONS

AD, Alzheimer's disease; RT, rivastigmine tartrate; CD, circular dichroism; FTIR, Fourier transform infrared spectroscopy; ITC, isothermal titration calorimetry

REFERENCES

(1) Clin, A. The Relationship between High-Fat Diet and Fibronectin Type-III Domain-Containing Protein 5 mRNA Expression. *Anatolian Clin.* **2018**, 1.

(2) Boström, P.; Wu, J.; Jedrychowski, M. P.; Korde, A.; Ye, L.; Lo, J. C.; Rasbach, K. A.; Boström, E. A.; Choi, J. H.; Long, J. Z.; et al. A PGC1-α-dependent myokine that drives brown-fat-like development of white fat and thermogenesis. *Nature* **2012**, *481*, 463.

(3) Zhang, Y.; Li, R.; Meng, Y.; Li, S.; Donelan, W.; Zhao, Y.; Qi, L.; Zhang, M.; Wang, X.; Cui, T.; et al. Irisin stimulates browning of white adipocytes through mitogen-activated protein kinase p38 MAP kinase and ERK MAP kinase signaling. *Diabetes* **2014**, *63*, 514−525.

(4) Wang, S.; Pan, J. Irisin ameliorates depressive-like behaviors in rats by regulating energy metabolism. *Biochem. Biophys. Res. Commun.* **2016**, *474*, 22−28.

(5) Qiao, X.; Nie, Y.; Ma, Y.; Chen, Y.; Cheng, R.; Yin, W.; Hu, Y.; Xu, W.; Xu, L. Irisin promotes osteoblast proliferation and differentiation via activating the MAP kinase signaling pathways. *Sci. Rep.* **2016**, *6*, No. 1.

(6) Colaianni, G.; Cuscito, C.; Mongelli, T.; Pignataro, P.; Buccoliero, C.; Liu, P.; Lu, P.; Sartini, L.; Di Comite, M.; Mori, G.; et al. The myokine irisin increases cortical bone mass. *Proc. Natl. Acad. Sci. U.S.A.* **2015**, *112*, 12157−12162.

(7) Piya, M. K.; Harte, A. L.; Sivakumar, K.; Tripathi, G.; Voyias, P. D.; James, S.; Sabico, S.; Al-Daghri, N. M.; Saravanan, P.; Barber, T. M.; et al. The identification of irisin in human cerebrospinal fluid: influence of adiposity, metabolic markers, and gestational diabetes. *Am. J. Physiol.: Endocrinol. Metab.* **2014**, *306*, E512−E518.

(8) Dun, S. L.; Lyu, R.-M.; Chen, Y.-H.; Chang, J.-K.; Luo, J. J.; Dun, N. J. Irisin-immunoreactivity in neural and non-neural cells of the rodent. *Neuroscience* **2013**, *240*, 155−162.

(9) Li, D.-J.; Li, Y.-H.; Yuan, H.-B.; Qu, L.-F.; Wang, P. The novel exercise-induced hormone irisin protects against neuronal injury via activation of the Akt and ERK1/2 signaling pathways and contributes to the neuroprotection of physical exercise in cerebral ischemia. *Metabolism* **2017**, *68*, 31−42.

(10) Okonkwo, O. C.; Schultz, S. A.; Oh, J. M.; Larson, J.; Edwards, D.; Cook, D.; Koscik, R.; Gallagher, C. L.; Dowling, N.; Carlsson, C. M.; et al. Physical activity attenuates age-related biomarker alterations in preclinical AD. *Neurology* **2014**, *83*, 1753−1760.

(11) Walker, J. M.; Klakotskaia, D.; Ajit, D.; Weisman, G. A.; Wood, W. G.; Sun, G. Y.; Serfozo, P.; Simonyi, A.; Schachtman, T. R. Beneficial effects of dietary EGCG and voluntary exercise on behavior in an Alzheimer's disease mouse model. *J. Alzheimer's Dis.* **2015**, *44*, 561−572.

(12) Kim, O. Y.; Song, J. The role of irisin in Alzheimer's disease. *J. Clin. Med.* **2018**, *7*, 407.

(13) Erickson, K. I.; Weinstein, A. M.; Lopez, O. L. Physical activity, brain plasticity, and Alzheimer's disease. *Arch. Med. Res.* **2012**, *43*, 615−621.

(14) Lourenco, M. V.; Frozza, R. L.; de Freitas, G. B.; Zhang, H.; Kincheski, G. C.; Ribeiro, F. C.; Gonçalves, R. A.; Clarke, J. R.; Beckman, D.; Staniszewski, A.; et al. Exercise-linked FNDC5/irisin rescues synaptic plasticity and memory defects in Alzheimer's models. *Nat. Med.* **2019**, *25*, 165.

(15) Noda, Y.; Kuzuya, A.; Tanigawa, K.; Araki, M.; Kawai, R.; Ma, B.; Sasakura, Y.; Maesako, M.; Tashiro, Y.; Miyamoto, M.; et al. Fibronectin type III domain-containing protein 5 interacts with APP and decreases amyloid β production in Alzheimer's disease. *Mol. Brain* **2018**, *11*, 61.

(16) Winblad, B.; Machado, J. C. Use of rivastigmine transdermal patch in the treatment of Alzheimer's disease. *Expert Opin. Drug Delivery* **2008**, *5*, 1377−1386.

(17) Pan, Y.; Xu, X.; Wang, X. Rivastigmine blocks voltage-activated K+ currents in dissociated rat hippocampal neurons. *Br. J. Pharmacol.* **2003**, *140*, 907−912.

(18) Bar-On, P.; Millard, C.; Harel, M.; Dvir, H.; Enz, A.; Sussman, J.; Silman, I. Kinetic and structural studies on the interaction of cholinesterases with the anti-Alzheimer drug rivastigmine. *Biochemistry* **2002**, *41*, 3555−3564.

(19) Agrawal, R.; Siddiqi, M. K.; Thakur, Y.; Tripathi, M.; Asatkar, A. K.; Khan, R. H.; Pande, R. Explication of bovine serum albumin binding with naphthyl hydroxamic acids using a multispectroscopic and molecular docking approach along with its antioxidant activity. *Luminescence* **2019**, 628−643.

(20) Shamsi, A.; Anwar, S.; Mohammad, T.; Alajmi, M. F.; Hussain, A.; Rehman, M.; Hasan, G. M.; Islam, A.; Hassan, M. MARK4 Inhibited by AChE Inhibitors, Donepezil and Rivastigmine Tartrate: Insights into Alzheimer's Disease Therapy. *Biomolecules* **2020**, *10*, 789.

(21) Spencer, C. M.; Noble, S. Rivastigmine. *Drugs Aging* **1998**, *13*, 391−411.

(22) Jann, M. W. Rivastigmine, a new-generation cholinesterase inhibitor for the treatment of Alzheimer's disease. *Pharmacotherapy* **2000**, *20*, 1−12.

(23) Desai, A.; Grossberg, G. Review of rivastigmine and its clinical applications in Alzheimer's disease and related disorders. *Expert Opin. Pharmacother.* **2001**, *2*, 653−666.

(24) Lourenco, M. V.; Frozza, R. L.; de Freitas, G. B.; Zhang, H.; Kincheski, G. C.; Ribeiro, F. C.; Gonçalves, R. A.; Clarke, J. R.; Beckman, D.; Staniszewski, A.; et al. Exercise-linked FNDC5/irisin rescues synaptic plasticity and memory defects in Alzheimer's models. *Nat. Med.* **2019**, *25*, 165−175.

(25) Leader, B.; Baca, Q. J.; Golan, D. E. Protein therapeutics: a summary and pharmacological classification. *Nat. Rev. Drug Discovery* **2008**, *7*, 21−39.

(26) Orjuela, P.; González, I.; Osorio, L. Combination therapy as a strategy to prevent antimalarial drug resistance. *Biomedica* **2004**, *24*, 423−437.

(27) Broxterman, H. J.; Georgopapadakou, N. H. Anticancer therapeutics:"Addictive" targets, multi-targeted drugs, new drug combinations. *Drug Resist. Updates* **2005**, *8*, 183−197.

(28) Huang, S.-M.; Lertora, J. J.; Markey, S. P.; Atkinson, A. J., Jr. *Principles of Clinical Pharmacology*; Academic Press, 2012.

(29) Dinache, A.; Tozar, T.; Smarandache, A.; Andrei, I. R.; Nistorescu, S.; Nastasa, V.; Staicu, A.; Pascu, M.-L.; Romanitan, M. O. Spectroscopic Characterization of Emulsions Generated with a New Laser-Assisted Device. *Molecules* **2020**, *25*, 1729.

(30) Wang, B.-L.; Pan, D.-Q.; Zhou, K.-L.; Lou, Y.-Y.; Shi, J.-H. Multi-spectroscopic approaches and molecular simulation research of the intermolecular interaction between the angiotensin-converting enzyme inhibitor (ACE inhibitor) benazepril and bovine serum albumin (BSA). *Spectrochim. Acta, Part A* **2019**, *212*, 15−24.

(31) Wrann, C. D.; White, J. P.; Salogiannnis, J.; Laznik-Bogoslavski, D.; Wu, J.; Ma, D.; Lin, J. D.; Greenberg, M. E.; Spiegelman, B. M. Exercise induces hippocampal BDNF through a PGC-1α/FNDC5 pathway. *Cell Metab.* **2013**, *18*, 649−659.

(32) Soares, S.; Mateus, N.; De Freitas, V. Interaction of different polyphenols with bovine serum albumin (BSA) and human salivary α-amylase (HSA) by fluorescence quenching. *J. Agric. Food Chem.* **2007**, *55*, 6726−6735.

(33) Klajnert, B.; Stanisławska, L.; Bryszewska, M.; Pałecz, B. Interactions between PAMAM dendrimers and bovine serum albumin. *Biochim. Biophys. Acta, Proteins Proteomics* **2003**, *1648*, 115−126.

(34) Shamsi, A.; Ahmed, A.; Khan, M. S.; Al Shahwan, M.; Husain, F. M.; Bano, B. Understanding the binding between Rosmarinic acid and serum albumin: In vitro and in silico insight. *J. Mol. Liq.* **2020**, No. 113348.

(35) Mariam, J.; Dongre, P.; Kothari, D. Study of interaction of silver nanoparticles with bovine serum albumin using fluorescence spectroscopy. *J. Fluoresc.* **2011**, *21*, 2193.

(36) Lakowicz, J. R. Protein Fluorescence. In *Principles of Fluorescence Spectroscopy*; Springer, 1983; pp 341−381.

(37) Wang, Q.; Huang, C.-r.; Jiang, M.; Zhu, Y.-y.; Wang, J.; Chen, J.; Shi, J.-h. Binding interaction of atorvastatin with bovine serum

https://dx.doi.org/10.1021/acsomega.1c00517
ACS Omega 2021, 6, 7910−7921

albumin: Spectroscopic methods and molecular docking. *Spectrochim. Acta, Part A* **2016**, *156*, 155−163.
(38) Khan, S. N.; Islam, B.; Yennamalli, R.; Sultan, A.; Subbarao, N.; Khan, A. U. Interaction of mitoxantrone with human serum albumin: Spectroscopic and molecular modeling studies. *Eur. J. Pharm. Sci.* **2008**, *35*, 371−382.
(39) Kou, S.-B.; Lin, Z.-Y.; Wang, B.-L.; Shi, J.-H.; Liu, Y.-X. Evaluation of the binding behavior of olmutinib (HM61713) with model transport protein: Insights from spectroscopic and molecular docking studies. *J. Mol. Struct.* **2020**, *1224*, No. 129024.
(40) Lineweaver, H.; Burk, D. The determination of enzyme dissociation constants. *J. Am. Chem. Soc.* **1934**, *56*, 658−666.
(41) Alam, P.; Naseem, F.; Abdelhameed, A. S.; Khan, R. H. Effect of galactose on acid induced molten globule state of soybean agglutinin: biophysical approach. *J. Mol. Struct.* **2015**, *1099*, 149−153.
(42) Rehman, M. T.; Shamsi, H.; Khan, A. U. Insight into the binding mechanism of imipenem to human serum albumin by spectroscopic and computational approaches. *Mol. Pharmaceutics* **2014**, *11*, 1785−1797.
(43) Zhang, Y.-F.; Zhou, K.-L.; Lou, Y.-Y.; Pan, D.-q.; Shi, J.-H. Investigation of the binding interaction between estazolam and bovine serum albumin: multi-spectroscopic methods and molecular docking technique. *J. Biomol. Struct. Dyn.* **2017**, *35*, 3605−3614.
(44) Yousuf, M.; Shamsi, A.; Khan, P.; Shahbaaz, M.; AlAjmi, M. F.; Hussain, A.; Hassan, G. M.; Islam, A.; Rizwanul Haque, Q. M.; Hassan, M. Ellagic acid controls cell proliferation and induces apoptosis in breast cancer cells via inhibition of cyclin-dependent kinase 6. *Int. J. Mol. Sci.* **2020**, *21*, 3526.
(45) Kou, S.-B.; Lin, Z.-Y.; Wang, B.-L.; Shi, J.-H.; Liu, Y.-X., Evaluation of the binding behavior of olmutinib (HM61713) with model transport protein: Insights from spectroscopic and molecular docking studies. *J. Mol. Struct. 1224*, 129024.
(46) Wang, B.-L.; Kou, S.-B.; Lin, Z.-Y.; Shi, J.-H. Investigation on the binding behavior between BSA and lenvatinib with the help of various spectroscopic and in silico methods. *J. Mol. Struct.* **2020**, *1204*, No. 127521.
(47) Cahyana, Y.; Gordon, M. H. Interaction of anthocyanins with human serum albumin: Influence of pH and chemical structure on binding. *Food Chem.* **2013**, *141*, 2278−2285.
(48) Tripathi, T. Calculation of thermodynamic parameters of protein unfolding using far-ultraviolet circular dichroism. *J. Proteins Proteomics* **2013**, *4*, 85−91.
(49) Shamsi, A.; Al Shahwan, M.; Ahamad, S.; Hassan, M. I.; Ahmad, F.; Islam, A. Spectroscopic, calorimetric and molecular docking insight into the interaction of Alzheimer's drug donepezil with human transferrin: Implications of Alzheimer's drug. *J. Biomol. Struct. Dyn.* **2020**, *38*, 1094−1102.
(50) Watanabe, H.; Tanase, S.; Nakajou, K.; Maruyama, T.; Kragh-Hansen, U.; Otagiri, M. Role of Arg-410 and Tyr-411 in human serum albumin for ligand binding and esterase-like activity. *Biochem. J.* **2000**, *349*, 813−819.
(51) Zaidi, N.; Ajmal, M. R.; Rabbani, G.; Ahmad, E.; Khan, R. H. A comprehensive insight into binding of hippuric acid to human serum albumin: a study to uncover its impaired elimination through hemodialysis. *PLoS One* **2013**, *8*, No. e71422.
(52) Jedrychowski, M. P.; Wrann, C. D.; Paulo, J. A.; Gerber, K. K.; Szpyt, J.; Robinson, M. M.; Nair, K. S.; Gygi, S. P.; Spiegelman, B. M. Detection and quantitation of circulating human irisin by tandem mass spectrometry. *Cell Metab.* **2015**, *22*, 734−740.
(53) Lee, P.; Linderman, J. D.; Smith, S.; Brychta, R. J.; Wang, J.; Idelson, C.; Perron, R. M.; Werner, C. D.; Phan, G. Q.; Kammula, U. S.; et al. Irisin and FGF21 are cold-induced endocrine activators of brown fat function in humans. *Cell Metab.* **2014**, *19*, 302−309.
(54) Tripathi, T.; Röseler, A.; Rahlfs, S.; Becker, K.; Bhakuni, V. Conformational stability and energetics of Plasmodium falciparum glutaredoxin. *Biochimie* **2010**, *92*, 284−291.
(55) Ahmad, Z.; Ahmad, F. Physico-chemical characterization of products of unfolding of cytochrome c by calcium chloride. *Biochim. Biophys. Acta, Protein Struct. Mol. Enzymol.* **1994**, *1207*, 223−230.
(56) Ahmad, Z.; Yadav, S.; Ahmad, F.; Khan, N. Z. Effects of salts of alkali earth metals and calcium chloride on the stability of cytochrome c and myoglobin. *Biochim. Biophys. Acta, Protein Struct. Mol. Enzymol.* **1996**, *1294*, 63−71.
(57) Shamsi, A.; Mohammad, T.; Khan, M. S.; Shahwan, M.; Husain, F. M.; Rehman, M.; Hassan, M.; Ahmad, F.; Islam, A. Unraveling Binding Mechanism of Alzheimer's Drug Rivastigmine Tartrate with Human Transferrin: Molecular Docking and Multi-Spectroscopic Approach towards Neurodegenerative Diseases. *Biomolecules* **2019**, *9*, 495.
(58) Schumacher, M. A.; Chinnam, N.; Ohashi, T.; Shah, R. S.; Erickson, H. P. The Structure of Irisin Reveals a Novel Intersubunit β-Sheet Fibronectin Type III (FNIII) Dimer: Implications for Receptor Activation. *J. Biol. Chem.* **2013**, *288*, 33738−33744.
(59) Anwar, S.; Shamsi, A.; Kar, R. K.; Queen, A.; Islam, A.; Ahmad, F.; Hassan, M. I. Structural and biochemical investigation of MARK4 inhibitory potential of cholic acid: Towards therapeutic implications in neurodegenerative diseases. *Int. J. Biol. Macromol.* **2020**, 596−604.
(60) Shamsi, A.; Mohammad, T.; Anwar, S.; Alajmi, M. F.; Hussain, A.; Hassan, M. I.; Ahmad, F.; Islam, A. Probing the interaction of Rivastigmine Tartrate, an important Alzheimer's drug, with serum albumin: Attempting treatment of Alzheimer's disease. *Int. J. Biol. Macromol.* **2020**, *148*, 533−542.
(61) Shamsi, A.; Ahmed, A.; Khan, M. S.; Husain, F. M.; Amani, S.; Bano, B. Investigating the interaction of anticancer drug temsirolimus with human transferrin: Molecular docking and spectroscopic approach. *J. Mol. Recognit.* **2018**, *31*, No. e2728.
(62) Anwar, S.; Shamsi, A.; Shahbaaz, M.; Queen, A.; Khan, P.; Hasan, G. M.; Islam, A.; Alajmi, M. F.; Hussain, A.; Ahmad, F.; Hassan, M. I. Rosmarinic Acid Exhibits Anticancer Effects via MARK4 Inhibition. *Sci. Rep.* **2020**, *10*, No. 10300.
(63) Jacob, R. B.; Andersen, T.; McDougal, O. M. Accessible high-throughput virtual screening molecular docking software for students and educators. *PLoS Comput. Biol.* **2012**, *8*, No. e1002499.
(64) Trott, O.; Olson, A. J. AutoDock Vina: improving the speed and accuracy of docking with a new scoring function, efficient optimization, and multithreading. *J. Comput. Chem.* **2010**, *31*, 455−461.
(65) DeLano, W. *The PyMOL Molecular Graphics System*; DeLano Scientific: Palo Alto, CA, 2002.
(66) Biovia, D. S. *Discovery Studio Modeling Environment*; Dassault Systèmes: San Diego, 2015.
(67) Mohammad, T.; Mathur, Y.; Hassan, M. I. InstaDock: A single-click graphical user interface for molecular docking-based virtual high-throughput screening. *Briefings Bioinf.* **2020**, *26*, No. bbaa279.
(68) Hopkins, A. L.; Groom, C. R.; Alex, A. Ligand efficiency: a useful metric for lead selection. *Drug Discovery Today* **2004**, *9*, 430.

https://dx.doi.org/10.1021/acsomega.1c00517
ACS Omega 2021, 6, 7910−7921